Adsorption 2, 41–50 (1996)

Simulation of Adsorption of Liquid Mixtures of N_2 and O_2 in a Model Faujasite Cavity at 77.5 K

JUDE A. DUNNE AND ALAN L. MYERS
Department of Chemical Engineering, University of Pennsylvania, Philadelphia, PA 19104

DAVID A. KOFKE
Department of Chemical Engineering, State University of New York, Buffalo, NY 14260

Abstract. Grand canonical Monte Carlo simulations of adsorption of N_2 and O_2 and their mixtures in a model zeolitic cavity 14 Å in diameter were performed at 77.5 K for pressures ranging from zero up to saturation, where the adsorbed phase is in equilibrium with coexisting vapor and liquid phases. The same intermolecular potential functions were employed for gas-gas interactions in the vapor, liquid, and adsorbed phases. The gas-solid interaction potential includes dispersion-repulsion energy, induced electrostatic energy, and an ion-quadrupole term to model the interaction of the electric field in zeolites like NaX with polar molecules like N_2. The simulation of the coexisting vapor and liquid phases reproduces the saturation properties of pure liquid oxygen and nitrogen at 77.5 K. Activity coefficients in the adsorbed phase derived from simulations as a function of cavity filling and composition show negative deviations from Raoult's law, even though the non-idealities in the bulk liquid phase have the opposite sign. The simulation of the surface excess isotherm for adsorption from liquid mixtures exhibits preferential adsorption of N_2 and has the commonly-observed quadratic shape skewed toward the more strongly adsorbed component. Micropore condensation is observed for oxygen but not for nitrogen. The condensation of oxygen is similar to a first order phase transition but because of the small number of molecules that can fit into a micropore, coexistence of the two phases is replaced by oscillations between gas- and liquid-like densities.

Keywords: Monte Carlo simulation, Gibbs-Duhem integration, adsorption, liquid mixtures, faujasite

1. Introduction

The separation of liquid mixtures by adsorption is an alternative to distillation for solutions containing close-boiling isomers or heat-labile components. Central to further development in this field is the need for equations which describe and predict multicomponent liquid adsorption. Liquid adsorption may be divided into two categories:

1. Adsorption of dilute solutes from their solvents.
2. Adsorption of miscible liquids over the entire range of composition.

In the first case, existing theories predict multi-solute equilibrium from single-solute isotherms in a particular solvent. These theories, which are based upon constant activity of the solvent, apply when solute mole fractions are one percent or less.

In the second case, which is the subject of this paper, numerous theories have been proposed (Myers, 1989). If adsorbed-phase nonidealities are ignored, ideal adsorbed solution (IAS) theory may be used in conjunction with pure-vapor adsorption isotherms and vapor-liquid equilibrium data to predict multicomponent liquid adsorption. However, at the high coverages encountered in liquid adsorption, nonideal behavior is common. Theories which account for nonidealities are complicated and contain too many undetermined parameters; simpler theories with two or three parameters fit experimental data but the fitted parameters have no physical significance. What is needed is an equilibrium theory of adsorption from liquid mixtures

that strikes a balance between excessive complexity and over-simplification.

Molecular simulation has an important role to play in developing realistic and tractable theories. The molecular model accounts for the following effects:

1. Dispersion and repulsion interactions of adsorbate molecules with the walls of the micropores and with each other.
2. Partial exclusion of one species from some but not all of the micropores because of steric hindrance.
3. Energetic heterogeneity of the adsorbent due to its topology, and due to the presence of ions or partial charges on framework atoms of the adsorbent.
4. Nonideal behavior caused by differences in the interactions of polar and nonpolar molecules with the electric field inside the micropores.

Monte Carlo simulations based upon this molecular model yield equilibrium data for adsorption from liquid mixtures. These data are invaluable for checking the validity of various assumptions used in theories (ideal solution behavior, monolayer adsorption, etc.).

In the next section, the simulation techniques are described and the intermolecular potential parameters for both vapor-liquid equilibrium and vapor-adsorbed phase equilibrium are presented.

2. Molecular Model

A set of consistent potential parameters has been developed for the molecular simulation of all three phases: adsorbed, bulk liquid, and bulk vapor. First the intermolecular potentials and simulation technique for the bulk fluids (vapor and liquid) will be described and compared with experiment.

Bulk Fluids

Nitrogen and oxygen are modeled as single-site Lennard-Jones molecules with point quadrupoles. The intermolecular potential energies are assumed to be pairwise additive:

$$\Psi^{\text{gas-gas}} = \Psi^{\text{LJ}} + \Psi^{\text{QQ}} \tag{1}$$

where

$$\Psi^{\text{LJ}} = 4\epsilon\left[\left(\frac{\sigma}{r}\right)^{12} - \left(\frac{\sigma}{r}\right)^{6}\right] \tag{2}$$

and

$$\Psi^{\text{QQ}} = \frac{3Q_1Q_2}{4r_{12}^5}\left[1 - 5c_1^2 - 5c_2^2 - 15c_1^2c_2^2 + 2(c_{12} - 5c_1c_2)^2\right] \tag{3}$$

Here, Q_i is the quadrupole moment on the ith molecule, $c_i = \hat{e}_i \cdot \hat{r}_{12}$ and $c_{ij} = \hat{e}_i \cdot \hat{e}_j$. $\hat{r}_{12}$ is a vector joining the centers of molecules 1 and 2 and $\hat{e}_i$ is a unit vector along the quadrupole axis of molecule i. The values of quadrupole moments were taken from Gray and Gubbins (1984).

The potential parameters reported in Table 1 were optimized to agree with experimental vapor-liquid equilibrium data for oxygen and nitrogen. The basis for the pure component parameters (σ and ϵ) was correspondence with the experimental vapor pressure and liquid density. The vapor pressure is significant in this study because it is closely related to the chemical potential, which along with temperature is the most important state parameter in the adsorbed phase; liquid densities were chosen to ensure that appropriate molecular sizes were used in the model. Q^* is the reduced quadrupole moment:

$$Q^* = \frac{Q}{\sqrt{\epsilon\sigma^5}} \tag{4}$$

Values of the parameters in Table 1 are based on simulations of vapor-liquid equilibria at 77.5 K, which corresponds to a reduced temperature kT/ϵ much lower than any studied previously. We attempted to perform Gibbs ensemble simulations but found them to be unacceptable slow. Therefore a new method of evaluating phase equilibria by molecular simulation was adopted. This method, the Gibbs-Duhem integration technique (Kofke, 1993a, b), entails the simultaneous simulation of coexisting phases but does not require the particle exchanges which hamper the Gibbs ensemble method. Instead, it relies on the Clapeyron equation to ensure the equality of chemical potential in coexisting phases. An initial state of known coexistence is needed to begin the simulation. This was achieved by the usual Gibbs ensemble technique at the relatively high temperature

Table 1. Parameters of Lennard-Jones 12-6 potential and reduced quadrupole moment for gas-gas intermolecular energies.

Molecule	σ, Å	ϵ/k, K	Q^{*2}
Nitrogen	3.574	98.11	0.248
Oxygen	3.353	123.2	0.0222

Table 2. Comparison of properties of pure N_2 and O_2 at saturation with experiment (Sychev et al.; Jacobsen et al., 1986) at 77.5 K.

Molecule		Vapor pressure bar	Liquid density cm^3/mol	Heat of vaporization J/mol
Nitrogen	Experiment	1.033	34.8	5564
	Simulation	1.060	33.5	5568
Oxygen	Experiment	0.213	26.7	7163
	Simulation	0.218	26.1	7107

$kT/\epsilon = 1.0$. Gibbs-Duhem integration was then performed to traverse the saturation curve from this temperature down to the temperature of interest. About fifteen Gibbs-Duhem simulations of 10,000 production cycles and 5,000–10,000 relaxation cycles (where a cycle comprises one attempted translation and rotation per particle, and two volume changes) were performed for each pure component. The total number of particles used was 216, with above one-third of them in the vapor. As seen in Table 2, the agreement of the simulation with experimental data for vapor pressure and liquid density is remarkably good. Although the parameter optimization was based on vapor pressure and liquid density, the experimental heats of vaporization are also reproduced with errors less than 1%.

In the case of the binary mixture of N_2 and O_2 an additional degree of flexibility was introduced in the model through the cross-interaction energy parameter ϵ_{12}. The value of this parameter ($\epsilon_{12}/k = 113.35$ K) was chosen to fit experimental excess Gibbs free energy at 77.5 K (Pool et al., 1962) over the entire range of compositions. The geometric mean $\epsilon_{12}/k = \sqrt{\epsilon_{11}\epsilon_{22}}/k = 109.94$ K is unsatisfactory; minute changes in the value of ϵ_{12} have a large effect upon the excess Gibbs free energy. Gibbs-Duhem integration was performed along a locus through the mixture connecting pure, saturated N_2 with pure, saturated O_2. The fugacity fraction $\xi_{O_2} = f_{O_2}/(f_{N_2} + f_{O_2})$ determines the integration path, as detailed by Mehta and Kofke (1994). The simulation data generated for $\epsilon_{12} = 111.35$ K and the pure-component parameters in Table 1 are presented in Table 3.

Table 3. Simulation of vapor-liquid equilibria of binary mixtures of oxygen and nitrogen at 77.5 K. $\epsilon_{12}/k = 111.35$ K. ξ_{O_2} is the oxygen fugacity fraction and $(f_{O_2} + f_{N_2})$ is the sum of the fugacities.

	$f_{O_2} + f_{N_2}$	P	Mole fraction O_2	
ξ_{O_2}	bar	bar	Vapor	Liquid
0.00	1.000	1.060	0.000	0.000
0.05	0.870	0.918	0.051	0.178
0.10	0.762	0.802	0.099	0.330
0.15	0.672	0.705	0.149	0.459
0.20	0.599	0.624	0.204	0.545
0.25	0.541	0.561	0.251	0.628
0.30	0.489	0.507	0.303	0.691
0.35	0.448	0.464	0.351	0.741
0.40	0.412	0.425	0.402	0.793
0.45	0.381	0.392	0.450	0.820
0.50	0.354	0.365	0.500	0.851
0.55	0.331	0.339	0.552	0.880
0.60	0.310	0.317	0.598	0.902
0.65	0.292	0.298	0.648	0.919
0.70	0.275	0.280	0.693	0.935
0.75	0.261	0.264	0.751	0.949
0.80	0.247	0.251	0.800	0.961
0.85	0.236	0.239	0.851	0.971
0.90	0.225	0.228	0.901	0.982
0.95	0.215	0.218	0.951	0.991
1.00	0.206	0.211	1.000	1.000

Adsorbed Phase

The potential energy of an adsorbed molecule with the solid adsorbent, $\Psi^{\text{gas-solid}}$, was calculated by:

$$\Psi^{\text{gas-solid}} = \Psi^{\text{dr}} + \Psi^{\text{ind}} + \Psi^{\text{quad-ion}} \tag{5}$$

where Ψ^{dr}, Ψ^{ind}, and $\Psi^{\text{quad-ion}}$ are respectively the dispersion-repulsion, induced electrostatic, and quadrupole-ion energies.

The adsorbent is modelled as a spherical cavity. Interactions between atoms of the cavity wall and the adsorbate molecules are assumed to obey the Lennard-Jones 12-6 potential. If the adsorbent atoms are assumed to be uniformly distributed over the surface of the spherical cavity, the dispersion-repulsion portion of the gas-solid interaction energy is given by Soto and Myers (1981):

$$\Psi^{\text{dr}}_{\text{is}} = 4C\epsilon_{\text{is}}\left[\left(\frac{\sigma_{\text{is}}}{R}\right)^{12} L\left\{\frac{r^2}{R^2}\right\} - \left(\frac{\sigma_{\text{is}}}{R}\right)^{6} M\left\{\frac{r^2}{R^2}\right\}\right] \tag{6}$$

where

$$L\{x\} = \frac{(1 + 12x + 25.2x^2 + 12x^3 + x^4)}{(1-x)^{10}} \tag{7}$$

and

$$M\{x\} = \frac{(1+x)}{(1-x)^4} \tag{8}$$

Ψ_{is}^{dr} depends only on the radial distance r of the adsorbed molecule from the center of the cavity. The cavity radius R is taken to be 7.057 Å, a value used for NaX (Soto and Myers, 1981). The product $(C\epsilon_{is})$ and σ_{is} are, respectively, the energy and collision parameters for the interaction of molecule i with the wall of the cavity.

Many zeolites contain non-framework ions which serve to neutralize the net charge on an adsorbent structure. This net charge is due to the substitution of framework atoms with atoms of dissimilar valence, for example, Al for Si. These non-framework ions generate an electric field $\hat{E}$ within the cavity which interacts with the adsorbate molecules. This electric field at a given point is given by:

$$E^2 = E_x^2 + E_y^2 + E_z^2 \tag{9}$$

where

$$E_x = \sum_j q_j \frac{x_j - x}{r^3} \tag{10}$$

with similar expressions for E_y and E_z. q_j is the charge on the jth ion located at (x_j, y_j, z_j) and

$$r = \sqrt{(x_j - x)^2 + (y_j - y)^2 + (z_j - z)^2}$$

The induced electrostatic energy is given by:

$$\Psi^{ind} = -\frac{1}{2}\left[\alpha_i + \frac{1}{3}(\alpha_\parallel - \alpha_\perp)(3\cos^2\theta - 1)\right] E^2(r) \tag{11}$$

and the quadrupole-ion energy is given by:

$$\Psi^{quad\text{-}ion} = \frac{1}{2}\sum_j q_j Q_i \frac{(3\cos^2\theta - 1)}{r^3} \tag{12}$$

where α_i and $(\alpha_\parallel - \alpha_\perp)$ are the average polarizability and the internuclear polarizability, respectively. Q_i is the point quadrupole moment associated with molecule i. θ is the angle between the electric field $\hat{E}$ and the unit vector $\hat{e}$ that determines the orientation of the molecule.

Gas-solid potential parameters in Table 4 were calculated by means of the Lorentz-Berthelot mixing rules:

$$\sigma_{ik} = \sigma_{jk} + (\sigma_{ii} - \sigma_{jj}) \tag{13}$$

Table 4. Parameters for gas-solid dispersion-repulsion energy, Eq. (6), and polarizabilities. $\Delta\alpha = \alpha_\parallel - \alpha_\perp$.

Molecule	σ_{is}, Å	$C\epsilon_{is}/k$, K	$\alpha \times 10^{24}$ cm^3	$\Delta\alpha \times 10^{24}$ cm^3
Nitrogen	3.142	5000	1.74	0.696
Oxygen	3.031	5600	1.58	1.099

Table 5. Lennard-Jones 12-6 potential parameters for gas-sodium ion interactions.

Molecule	σ_{is}, Å	ϵ_{is}/k, K
Nitrogen	2.662	33.93
Oxygen	2.551	38.00

and

$$\epsilon_{ik} = \epsilon_{jk}\sqrt{\frac{\epsilon_{ii}}{\epsilon_{jj}}} \tag{14}$$

with a solid-solid collision diameter of 2.71 Å and an ion-ion collision diameter of 1.75 Å, both values having been taken from Bezus et al. (1978) in their work with NaX. The electric field was modeled by sodium ions with partial charges of 0.2 whose coordinates were obtained from Hseu (1972) for dehydrated NaX with a 1.4 ratio of Si/Al.

The dispersion parameters listed in Table 5 for interaction of the adsorbate molecules with the sodium ions were estimated from the Kirkwood-Müller equation and Eqs. (13) and (14). This interaction potential accounts for electron repulsion when adsorbate molecules approach the sodium ions.

3. Simulation of Adsorption

Grand canonical Monte Carlo (GCMC) simulations generated both pure component and mixture isotherms for the N_2—O_2 system. The independent variables of temperature, volume of adsorbent, and chemical potential, when fixed, allow the determination of the amount adsorbed and the heat of adsorption.

Adsorption Isotherms of Pure Vapors

The adsorption isotherms for pure components are shown in Fig. 1. The steep portion of the oxygen isotherm required 25×10^6 cycles for convergence; 4×10^6 cycles were sufficient for the other points. Each

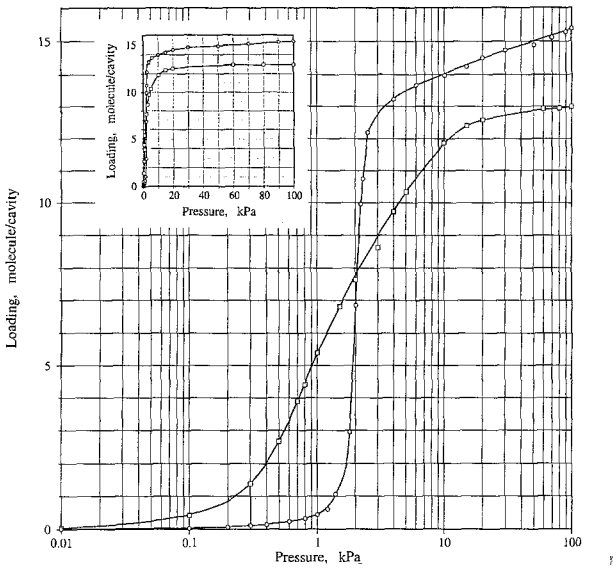

Figure 1. GCMC simulation of adsorption of pure N_2 (□) and O_2 (○) vapors in a zeolite cavity 14 Å in diameter at 77.5 K.

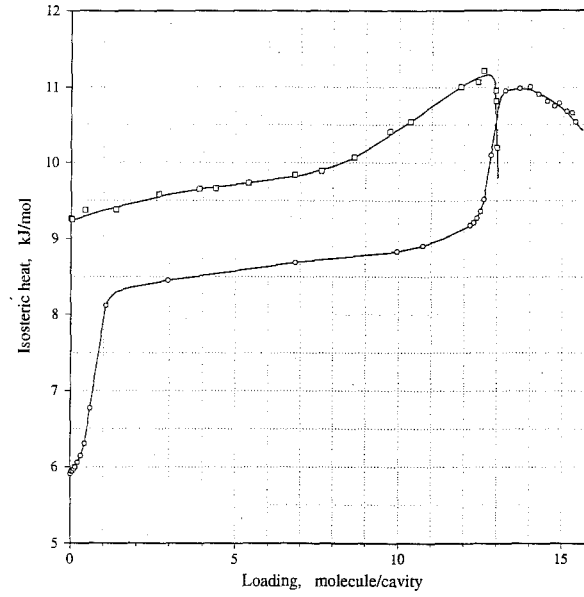

Figure 2. GCMC simulation of isosteric heat of adsorption of pure N_2 and O_2 vapors at 77.5 K.

cycle consists of an attempted displacement, creation, and destruction step. Statistics from the first 10% of each run were rejected to allow for equilibration.

The micropore capacities are about 13 and 15 molecules/cavity for nitrogen and oxygen, respectively. Since the thermodynamic system is so small, condensation from a gas to a liquid at the vapor pressure does not occur in the adsorbed phase. Although a first-order phase transition is impossible for 15 molecules, a phenomenon similar to condensation was found for the oxygen isotherm at a pressure of 2 kPa; this microcondensation effect is discussed later.

The Henry's law constants determined from three-dimensional integration for a single molecule in the cavity are 3.74 and 0.366 molecules/(cavity-kPa) for nitrogen and oxygen, respectively. These are the initial slopes of the adsorption isotherms on the inset of Fig. 1. The selectivity of the adsorbent for nitrogen relative to oxygen at the limit of zero pressure is the ratio of Henry's constants, or 3.74/0.366 = 11.1. The preferential adsorption of N_2 decreases with pressure until the adsorbed mixture becomes azeotropic above the crossover of the isotherms at 2 kPa.

Heats of Adsorption of Pure Vapors

The isosteric heats of adsorption determined from fluctuations in the energy and amount adsorbed are plotted on Fig. 2. The heats at zero coverage of 9.23 and 5.92 kJ/mol for N_2 and O_2, respectively, were determined by direct three-dimensional integration for one molecule in the cavity; these values agree with the simulation results shown in Fig. 2. The heat curve for N_2 shows an increase with loading indicative of cooperative interactions between adsorbate molecules.

The unusual heat curve for O_2 is a consequence of microcondensation. The small simulation system is, in principle, incapable of exhibiting the first-order phase transition associated with condensation of bulk fluids. Therefore the fact that 15 molecules exhibit a microcondensation effect which is very similar to condensation in bulk fluids is remarkable. Figure 3 shows the probability of occupation for various cavity fillings of O_2 determined from the simulation of the grand canonical ensemble. The microcondensation effect is apparent at the intermediate loading of about 7 molecules/cavity, where the average loading is least probable. The most probable occupation numbers are 0 or 13 molecules/cavity. The results were checked using different starting configurations to ensure condensation was not some pseudo equilibrium in which the molecules become trapped in a particular configuration. Also during the course of a simulation the occupation numbers in the cavity alternate

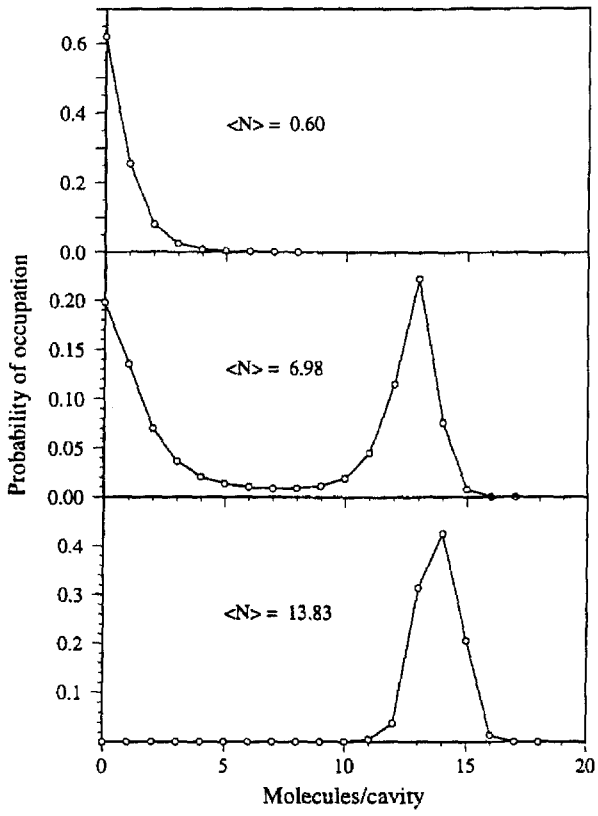

Figure 3. Probability of cavity occupation numbers determined from GCMC simulation of adsorption of O_2 vapor in zeolitic cavity 14 Å in diameter at 77.5 K. ⟨N⟩ is the GCMC average adsorption in molecules/cavity.

frequently between a low gas-like density and a high liquid-like density. At 13 molecules/cavity, the density of O_2 is very close to the density of the bulk liquid. The portion of the heat curve for O_2 in Fig. 2 from about 2 to 12 molecules/cavity is nearly constant because these occupation numbers are relatively improbable.

Figure 4 shows the probability of occupation for N_2 at an average filling of 6.88 molecules/cavity. N_2 shows no sign of condensation. The equilibrium configurations of the adsorbates in the cavity are the same for N_2 and O_2: 12–14 molecules adsorb on the surface of a spherical shell with their centers located about 3.9 Å from the center of the cavity; there is room for one additional molecule in the center of the cavity at high loading. The electric field inside the cavity has a maximum value of 3.4 V/nm adjacent to the sodium ions. The nitrogen molecules adsorb preferentially at sites adjacent to exposed sodium ions. If the quadrupole moment of nitrogen is "turned off", nitrogen exhibits

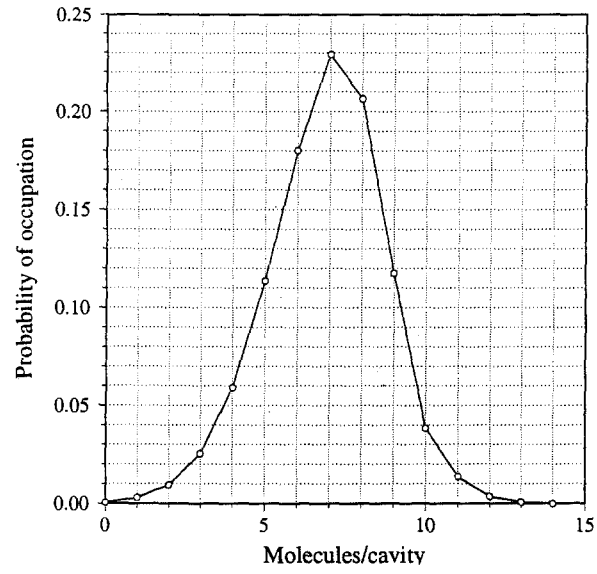

Figure 4. Probability of cavity occupation numbers determined from GCMC simulation of adsorption of N_2 vapor in zeolite cavity 14 Å in diameter at 77.5 K. The GCMC average adsorption is 6.88 molecules/cavity.

the same microcondensation. Thus the strong electrostatic interaction of nitrogen molecules with the surface inhibits condensation.

Adsorption of Gas Mixtures

The vapor-adsorbed phase and vapor-liquid phase equilibria for binary mixtures of N_2 and O_2 are plotted on Fig. 5. Mixture simulations were run for longer Markov chains: 40×10^6 cycles with the first 5% rejected for equilibration. The dashed line is the vapor-adsorbed phase equilibrium at the limit of zero pressure, based on the selectivity for N_2 relative to O_2 (11.1) predicted by the ratio of Henry's constants. Vapor-adsorbed phase equilibria are also given for three isobars: 0.8, 2.0, and 4.0 kPa. The preferential adsorption of N_2 decreases with increasing pressure as predicted by the intersection of the isotherms (see Fig. 1) at 2 kPa.

The isotherm for adsorption from the liquid phase was determined using the fugacities of N_2 and O_2 at saturation in Table 3 as independent variables for the GCMC simulation. The composition of the azeotrope is 53 mole percent N_2.

The vapor-liquid equilibrium diagram is also plotted on Fig. 5 using the simulation data in Table 3. N_2 is preferentially adsorbed but is the lighter component in the liquid phase.

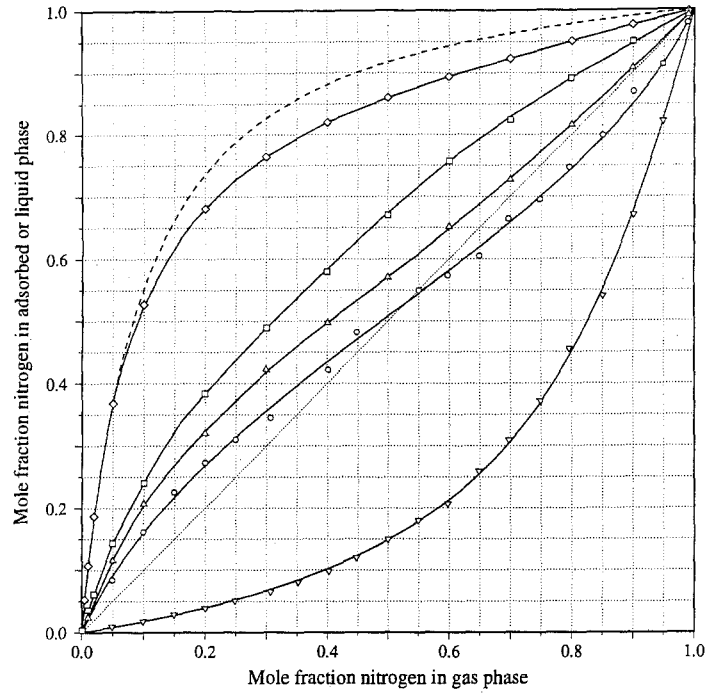

Figure 5. Phase diagrams for mixtures of N_2 and O_2 at 77.5 K from GCMC simulations. Dashed line for the limit of zero pressure is based upon the ratio of Henry's constants (11.1). Adsorption isobars are for 0.8 kPa (◇), 2.0 kPa (□), 4.0 kPa (△), and vapor simulation (○). The vapor-liquid equilibria (▽) were taken from the simulation data in Table 3.

The thermodynamic consistency of the isotherm at saturation was tested by the equation (Myers, 1989):

$$\int_{f=0}^{f_1^s} \frac{n_1}{f}\,df - \int_{f=0}^{f_2^s} \frac{n_2}{f}\,df = \int_{x_1=0}^{1} \frac{n_1^e}{\gamma_1 x_1 x_2}\,d(\gamma_1 x_1) \tag{15}$$

where n is the amount adsorbed, f is the vapor fugacity, f^s is the vapor fugacity at saturation, x is the mole fraction in the liquid phase, and γ is the activity coefficient in the liquid phase. n_1^e is the surface excess of component 1 in the adsorbed phase discussed below. Identifying N_2 and O_2 as component nos. 1 and 2, respectively, numerical integration of the simulation data according to Eq. (15) yields:

$$54.83 - 33.36 \approx 21.57$$

The less than 1% error between the right- and left-hand sides of the equation indicates that the simulation data for the pure-vapor isotherm and their mixtures are thermodynamically consistent.

Surface Excess for Adsorption from Liquid Phase

The surface excess for adsorption from the bulk liquid phase at saturation was calculated from the simulation data at saturation by (Valenzuela et al., 1989):

$$n_1^e = n_1 x_2 - n_2 x_1 \tag{16}$$

where n_1 and n_2 are the amounts adsorbed of N_2 and O_2, respectively, and x is the mole fraction in the bulk liquid phase. Experimentally, the surface excess of component i is determined from a material balance as the amount of i in the bulk liquid solution before adding the adsorbent, minus the amount of i remaining in the bulk liquid solution at equilibrium. The surface excess is zero if the composition of the adsorbed and liquid phases are equal.

The simulated surface excess isotherm from Eq. (16) is plotted on Fig. 6 as a function of the liquid-phase composition. N_2 is selectively adsorbed from the liquid; the maximum surface excess of 5 molecules/cavity occurs at a liquid composition of 20% N_2. The quadratic shape skewed toward the more strongly adsorbed

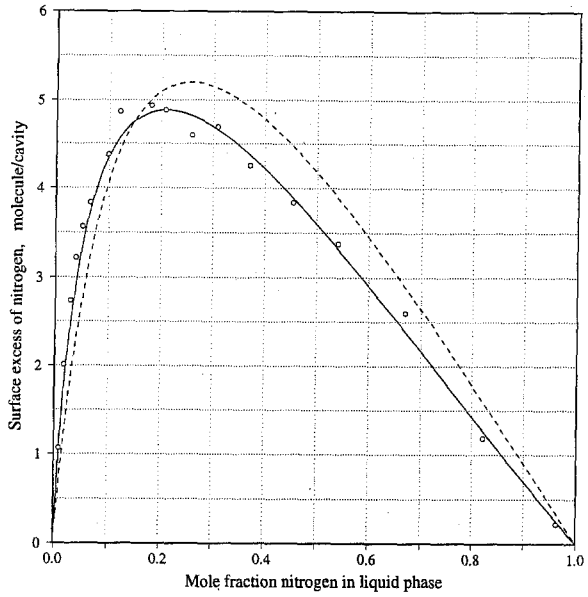

Figure 6. GCMC simulation of surface excess for preferential adsorption of N_2 from liquid mixtures of N_2 and O_2 in a zeolitic cavity 14 Å in diameter at 77.5 K. The solid lines is Eq. (18) for the parameters $P_2^\circ/P_1^\circ = 1.0$, $C' = -0.547$, and the constants in Table 6. The dashed line is the prediction for an ideal adsorbed solution ($C' = 0$).

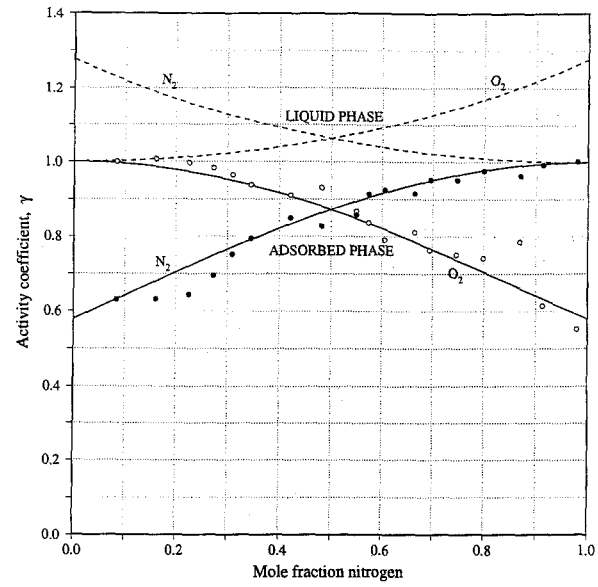

Figure 7. Activity coefficients in adsorbed phase (solid lines) and liquid phase (dashed lines) at 77.5 K from simulations. The points plotted for the adsorbed phase were calculated from the GCMC simulation of adsorption along the saturated-vapor locus.

component typical for surface excess isotherms is observed here also.

4. Theory

The activity coefficients obtained from simulation data are plotted on Fig. 7 for the liquid phase and for the adsorbed phase at saturation. In both cases the curves for the activity coefficients are symmetric in composition and, within the accuracy of the simulations, obey the one-constant equations $\ln \gamma_1 = Cx_2^2$ and $\ln \gamma_2 = Cx_1^2$. The values are $C = 0.244$ for the liquid phase and $C' = -0.547$ for the adsorbed phase. Thus the bulk liquid has small positive deviations from Raoult's law and the adsorbed phase has negative deviations from Raoult's law. The difference between the nonidealities in the adsorbed and liquid phases is caused by the solid, which exerts an influence upon the equilibrium configurations of the adsorbate molecules depending upon differences in their size and polarity.

The activity coefficients are unity at the limit of zero pressure and the nonideality of the adsorbed phase increases as the pressure approaches saturation. The activity coefficients were fitted by the empirical equation (Talu et al., 1995):

$$\frac{g^e}{RT} = Cx_1'x_2'(1 - e^{\beta\psi}) \tag{17}$$

where g^e is the excess Gibbs free energy of the adsorbed phase, x' is the mole fraction in the adsorbed phase, and $\psi = \Pi A/RT$. The quantity Π is the spreading pressure of the adsorbed solution, but ψ is the thermodynamic variable given by the integrals in Eq. (15). The two constants $C = -0.547$ and $\beta = 0.175$ (molecule/cavity)$^{-1}$ reproduce the vapor-adsorbed phase equilibria plotted on Fig. 5, including the azeotrope at saturation.

An equation for the surface excess (Myers, 1989) that is simple in form but has general validity is:

$$n_1^e = \frac{x_1x_2(K_{12} - 1)}{x_1K_{12}/m_1 + x_2/m_2} \tag{18}$$

where

$$K_{12} = K_{12}^\circ\left(\frac{\gamma_1\gamma_2'}{\gamma_2\gamma_1'}\right) \tag{19}$$

and

$$K_{12}^\circ = \frac{P_2^\circ P_1^s}{P_1^\circ P_2^s} \tag{20}$$

Table 6. Constants in Eq. (18) for surface excess.

Molecule	m_i molecules/cavity	P_i^s kPa
Nitrogen	12.3	106
Oxygen	14.9	21.8

where x is the mole fraction in the liquid, γ_i is the activity coefficient of component i in the liquid phase, and γ_i' is the activity coefficient of component i in the adsorbed phase.

The activity coefficients in the adsorbed phase γ' in Eq. (19) are functions of the composition of the adsorbed phase x'. Since the independent variable is the composition of the liquid phase, x' is unknown and must be determined by numerical solution of the equation:

$$x_1' = \frac{x_1 K_{12}}{x_1 K_{12} + x_2} \tag{21}$$

This is similar to an isothermal dew-point calculation for vapor-liquid equilibrium, for which the activity coefficients are a explicit function of the unknown liquid-phase composition.

The vapor pressures and saturation capacities needed in Eq. (18) are listed in Table 6. The activity coefficients in the liquid phase are known from the vapor-liquid equilibria: in this case by the equations $\ln \gamma_1 = Cx_2^2$ and $\ln \gamma_2 = Cx_1^2$, with $C = 0.244$. Generally activity coefficients for the adsorbed phase are unknown, so a similar constant C' for the adsorbed phase is needed. A second unknown in Eq. (18) is the ratio of adsorbate vapor pressures P_2°/P_1°. These two constants were evaluated by a best fit of Eq. (18) to the simulation data plotted in Fig. 6. The result is $C' = -0.547$ and $P_2^\circ/P_1^\circ = 1$. Therefore $K_{12}^\circ = P_1^s/P_2^s = 4.86$. The values for these constants agree with the vapor-adsorbed phase equilibria discussed previously: the adsorbed-phase activity coefficients are those predicted by Eq. (17), and the ratio of adsorbate vapor pressures (unity) is the average value at saturation of the vapor. Thus the fitted parameters have physical significance.

The theory behind Eq. (18) assumes that the ratio of vapor pressures P_2°/P_1° is constant along the saturation curve. This is strictly untrue but a satisfactory approximation. The second assumption that adsorption near saturation is constant is supported by the isotherms plotted in the inset of Fig. 1.

5. Summary and Conclusions

Simulations were performed at 77.5 K for the pure components and mixtures of N_2 and O_2 in a zeolitic cavity 14 Å in diameter. The adsorption isotherms were determined from zero pressure up to saturation, where the adsorbed phase is in equilibrium with coexisting liquid and vapor phases. The same intermolecular potential functions were used for gas-gas interactions in the vapor phase, liquid phase, and adsorbed phase. The gas-solid potential energy includes an ion-quadrupole term to model the interaction of the electric field in zeolites like NaX with polar molecules like N_2. N_2 has a large quadrupole moment compared to O_2, but the potential contribution from dispersion is larger for O_2 than for N_2. Therefore the adsorbent selectively adsorbs N_2, but O_2 is the heavy component in the bulk liquid phase.

The single-gas isotherms are cooperative in nature, as indicated by the increase in the heat of adsorption with cavity filling. The oxygen displays a microcondensation effect at a reduced temperature $T^* = kT/\epsilon = 0.63$ in which intermediate loadings oscillate between an empty cavity and a full cavity. Since the system is small (about 15 molecules), the distribution of cavity occupation numbers is continuous. The quadrupole of N_2 prevents such microcondensation

Adsorbed mixtures of N_2 and O_2 display the negative deviations from Raoult's law commonly observed experimentally, even though nonidealities in the bulk liquid phase have the opposite sign.

The empirical Eq. (17) provides an accurate representation of nonidealities in the adsorbed phase over the entire region of cavity filling from zero pressure to saturation.

Acknowledgment

This research was supported by a grant (NSF CTS 9213832) from the National Science Foundation.

References

Bezus, A.G., A.V. Kiselev, A.A. Lopatkin, and P.Q. Du, "Molecular statistical calculation of the thermodynamic adsorption characteristics of zeolites using the atom-atom approximation, Part 1: Adsorption of methane by zeolite NaX," *J. Chem. Soc. Faraday Trans. 2*, **74**, 367–379 (1978).

Gray, C.G. and K.E. Gubbins, *Theory of Molecular Fluids*, Oxford, Clarendon Press, 1984.

Hseu, T.H., Ph.D. Dissertation, University of Washington, 1972.

Jacobsen, R.T., R.B. Stewart, and M. Jahangiri, "Thermodynamic properties of nitrogen from the freezing line to 2000 K at pressure to 1000 MPa," *J. Phys. Chem. Ref. Data*, **15**(2), 735–909 (1986).

Karavias, F. and A.L. Myers, "Monte Carlo simulations of adsorption of non-polar and polar molecules in zeolite X," *Molec. Sim.*, **8**, 23–50 (1991).

Kofke, D.A., "Direct evaluation of phase coexistence by molecular simulation via integration along the saturation line," *J. Chem. Phys.*, **98**(5), 4149–4162 (1993).

Kofke, D.A., "Gibbs-Duherm integration: A new method for direct evaluation of phase coexistence by molecular simulation," *Mol. Phys.*, **78**(6), 1331–1336 (1993).

Mehta, M. and D.A. Kofke, "Coexistence diagrams of mixtures by molecular simulation," *Chem. Eng. Sci.*, **49**, 2633–2645 (1994).

Myers, A.L., "Equation for equilibrium adsorption from liquid mixtures," *Fundamentals of Adsorption*, A.B. Mersmann and S.E. Scholl (Eds.), Engineering Foundation, New York, 609–618 (1989).

Pool, R.A.H., G. Saville, T.M. Herrington, B.D.C. Shields, and L.A.K. Staveley, "Some excess thermodynamic functions for the liquid systems Argon + Oxygen, Argon + Nitrogen, Nitrogen + Oxygen, Nitrogen + Carbon Monoxide, and Argon + Carbon Monoxide," *Trans. Faraday Soc.*, **58**, 1692–1704 (1962).

Smit, B. and C.P. Williams, "Vapor-liquid equilibria for quadrupolar Lennard-Jones fluids," *J. Phys. Condens. Matter*, **2**, 4281–4288 (1990).

Soto, J.L. and A.L. Myers, "Monte Carlo studies of adsorption in molecular sieves," *Mol. Phys.*, **42**, 971–983 (1981).

Stapleton, M.D., D.J. Tildesley et al., "Phase equilibria of quadrupolar fluids by simulation in the Gibbs ensemble," *Molec. Sim.*, **2**, 147–180 (1989).

Sychev, V.V., A.A. Vasserman, A.D. Kozlov, G.A. Spiridonov, and V.A. Tsymarny, *Thermodynamic Properties of Oxygen*, National Standard Reference Data Service of the USSR: A Series of Proprietary Tables, Hemisphere Publishing, New York (1987).

Talu, O., J. Li, and A.L. Myers, "Activity coefficients of adsorbed mixtures," *Adsorption*, **1**(2), 103–112 (1995).

Valenzuela, D. and A.L. Myers, *Adsorption Equilibrium Data Handbook*, Prentice-Hall, Englewood-Cliffs, N.J. (1989).